

# Renormalization group approach to unified description of continuous and the first order phase transitions: application to the Blume-Capel model

V. I. Tokar<sup>1,2</sup>

<sup>1</sup>Université de Strasbourg, CNRS, IPCMS, UMR 7504, F-67000 Strasbourg, France

<sup>2</sup>G. V. Kurdyumov Institute for Metal Physics of the N.A.S. of Ukraine, 36 Acad. Vernadsky Boulevard, UA-03142 Kyiv, Ukraine

**Abstract.** The renormalization group (RG) equation in the self-consistent local potential approximation (SC-LPA) suggested earlier for the description of continuous phase transitions in lattice models of the Landau-Ginzburg type has been applied to the solution of the spin-1 Blume-Capel model on the simple cubic lattice. The calculated transition temperatures of both continuous and the first-order phase transitions (FOPTs) in zero external field have been found to be in excellent agreement with the best available estimates. It has been argued that the SC-LPA RG equation may give more accurate and complete description of the FOPTs than those reported in alternative approaches. It has been shown that the SC-LPA RG equation can be cast in the form of the generalized Burgers' equation (GBE). In this formulation of the RG the FOPTs have been shown to assume the form of the shock-wave solutions of GBE in the inviscid limit. Universality of the RG flow in the vicinity of the fixed point describing FOPTs has been discussed.

*Keywords:* nonperturbative renormalization group, local potential approximation, Burgers' equation, Blume-Capel model, tricritical point, first order phase transitions, phase transition temperatures

## 1. Introduction

From statistical-mechanical standpoint phase transitions are nonperturbative phenomena because they are formally defined as singularities in the dependence of the free energy (FE) on thermodynamic parameters whereas the microscopic Hamiltonians at the transition points are analytic. Thus, the singularities cannot appear in a finite order of a perturbative expansion and should be sought as the points of divergence of the series. In field-theoretic models of the Landau-Ginzburg type high order perturbative expansions are notoriously difficult [1] so numerous alternative techniques have been developed to describe phase transitions.

The most systematic approaches are based on the Monte Carlo (MC) simulations [2] and the temperature series expansions (TSE) [3, 4]. However, reliable quantitative results can be obtained within these techniques only at the cost of large-scale numerical and/or analytic calculations which still do not guarantee good accuracy because of the absence of reliable convergence criteria. For example, in [5] the MC simulations in the box containing more than a billion of lattice sites performed during more than two thousand CPU core years did not reproduce the critical exponent of the specific heat with acceptable precision. Only one critical point was investigated in this study so if one needs to deal with continuous lines of phase transitions the computations may become prohibitively lengthy.

Such a situation is met in the Blume-Capel model (BCM) [6, 7] where phase transitions comprise three lines of critical points, one line of the first order phase transitions (FOPTs) and a tricritical point (TCP) (see, e.g., figure 1 in [4]). For dealing with such cases many computationally undemanding heuristic approaches have been developed for studies where numerical accuracy is not a major priority (see, e.g., [8, 9, 10, 11, 12, 13, 14, 15] and references therein). Among them, the most prospective from the standpoint of the unified description of phase transitions of all kinds seems to be those based on the nonperturbative renormalization group (NPRG) (see bibliography of in review papers [16, 17]). The main reason for this is that such fundamental features of the continuous phase transitions as the universality and the scaling laws are intrinsic to the RG while even in the most rigorous alternative approaches their validity is not guaranteed and severe violations may take place even in large-scale simulations [18, 5]. Besides, FOPTs are arguably simpler than the continuous transitions [19, 20, 9] so the task of describing FOPTs within NPRG approach seems to be more feasible than the incorporation of realistic critical behaviour into, e.g., the cluster methods [8, 10, 13] efficient in the description of FOPTs.

This viewpoint was implemented in [9] with some success. The RG equation used by the authors allowed them to calculate with a good accuracy the critical temperature and to eliminate the van der Waals loops that plague mean field (MF) theories of FOPTs. This ensued in the correct prediction of the infinite susceptibility in the coexistence region but the discontinuity in the inverse susceptibility at the region boundaries in three dimensional (3d) case could not be reproduced [9]. Besides, the calculated critical

exponents did not agree well with known values. Nevertheless, the results show that NPRG is a viable approach to the problem of simultaneous description of the continuous phase transitions and the FOPTs while the cause of difficulties encountered in [9] should be sought in deficiencies of NPRG implementation because the approach in itself is exact [19].

The aim of the present paper is to apply to the problem of unified description of phase transitions of all kinds the RG equation derived in [21, 22, 15]. As in [9], it was based on the local potential approximation (LPA) [19, 23, 24, 16, 25, 26] but was derived within different—“layer-cake”—renormalization scheme. The approach proved to be efficient in calculating critical temperatures and other non-universal quantities in 3d spin-lattice models [22, 15]; besides, the critical exponents better agreed with the known values than in [9].

In the present paper it will be shown that an advantage of the RG equation of [21, 22, 15] is that it can be cast in the form of the generalized Burgers’ equation [27] with time-dependent viscosity. The FOPTs in this formalism appear as the shock wave solutions when the equation becomes inviscid. This results in the infinite susceptibility in the coexistence region and in the appearance of the discontinuities of the inverse susceptibility at the region boundaries. The quantitative accuracy of the theory will be tested on the spin-1 BCM on the simple cubic (sc) lattice [6, 7]. This choice was motivated by the fact that the solution of BCM in the MF approximation (see Appendix A in [4]) qualitatively reproduces the phenomenology of the extended Landau-Ginzburg model [28]. The latter along with the usual quartic ( $\phi^4$ ) term [28, 19] contains the sixth order term ( $\phi^6$ ) which makes possible to describe in addition to the conventional critical behaviour also the tricritical point and the FOPTs. For our purposes the advantage of BCM in comparison with the Landau-Ginzburg model is that because of the spin-lattice nature of BCM there exists a wealth of quantitative data obtained in MC simulations and in TSE (see extensive bibliography and TSE solutions in [4]) needed in quantitative comparison.

## 2. The model and the RG formalism

In notation of [7, 29, 30] the Hamiltonian of the ferromagnetic BCM in zero external field reads

$$\mathcal{H} = -J \sum_{\langle ij \rangle} s_i s_j + D \sum_i s_i^2 \quad (1)$$

where  $J > 0$  is the interaction between nearest neighbour (nn) spin-1 Ising spins; subscripts  $i, j$  denote the sites of the sc lattice of size  $N$ ; the summation in the first term on the right hand side (r.h.s.) is over nn pairs and  $D$  is the crystal field splitting [6, 7] or the anisotropy field [4, 30].

To simplify notation, (1) is convenient to cast in the form

$$H = \frac{\mathcal{H}}{T} = -K \sum_{\langle ij \rangle} s_i s_j + \Delta \sum_i s_i^2$$

$$= \frac{1}{2} \sum_{ij} (\hat{\epsilon}_{ij} + r\delta_{ij}) s_i s_j + \left( \Delta - \frac{qK+r}{2} \right) \sum_i s_i^2. \quad (2)$$

where temperature  $T$  is assumed to be measured in energy units:  $T = k_B T^{(K)}$  ( $T^{(K)}$  the temperature in Kelvins). Besides,  $J$  will be chosen as the energy unit so in (2)  $K = 1/T$  and  $\Delta = D/T$ . Matrix  $\hat{\epsilon}$  in (2) is defined as

$$\hat{\epsilon} = [qK\delta_{ij} - K_{ij}], \quad (3)$$

where  $q$  is the coordination number equal to 6 for the sc lattice,  $K_{ij}$  is equal to  $K$  when  $i$  and  $j$  are nn sites and to zero otherwise. The form of  $\hat{\epsilon}$  in (3) has been chosen for convenience of comparison with the RG theory dealing with the Fourier components [19] in the long wavelength limit

$$\epsilon(\mathbf{k})_{k \rightarrow 0} \propto k^2 \quad (4)$$

where  $\mathbf{k}$  is the lattice Fourier momentum. With similar purpose an arbitrary parameter  $r$  has been introduced in (2) in order that the inverse of the matrix in the parentheses in the first term on the second line in (2)  $\hat{G} = (\hat{\epsilon} + r)^{-1}$  under the lattice Fourier transform took the form [22, 15]

$$G(\mathbf{k}) = \frac{1}{\epsilon(\mathbf{k}) + r}. \quad (5)$$

The fluctuating field is introduced in the formalism by replacing the trace over the discrete spins  $s_i = 0, \pm 1$  in the BCM partition function by  $N$ -dimensional integral over the continuous spins  $-\infty < s_i < \infty$  as

$$Z[h] = \int \dots \int e^{-H + \sum_i h_i s_i} \prod_l ds_l [\delta(s_l) + 2\delta(s_l^2 - 1)], \quad (6)$$

where interaction with the source field  $h$  has been separated from Hamiltonian because it will be necessary for derivation of thermodynamic relations, in particular, in the Legendre transforms.

Next with the use of  $N$ -dimensional Gaussian integral and the shift operator [31, 10, 15, 22] the partition function can be cast in the form

$$Z[h] = \exp\left(\frac{1}{2} h \hat{G} h\right) R[\hat{G}h] \quad (7)$$

where

$$R[s] = \exp\left(\frac{1}{2} \partial_s \hat{G} \partial_s\right) \exp\left(-\sum_i u^b(s_i)\right). \quad (8)$$

The unrenormalized (“bare”) local potential in this expression is defined as

$$\begin{aligned} \exp[-u^b(s_i)] &= [\det(2\pi\hat{G})]^{1/2N} \\ &\times \exp\left[-\left(\Delta - \frac{qK+r}{2}\right) s_i^2\right] [\delta(s_i) + 2\delta(s_i^2 - 1)] \end{aligned} \quad (9)$$

where use has been made of (2) and (6).

### 2.1. Self-consistent RG equation

Because the bare potential in (9) is site-local, the BCM can be solved by the SC-LPA RG approach [15, 22] based on the differential equation

$$u_t = \frac{1}{2} [p(t)u_{xx} - u_x^2]. \quad (10)$$

where  $u(x, t)$  is the local potential that depends on the evolution parameter  $t$  which defines the stage of the “layer-cake” renormalization (see figure 1) and on the local field  $x$ . The subscripts  $t$  and  $x$  denote partial derivatives and

$$p(t) = \rho_{tot}(t^{-1} - r) = \int_0^{t^{-1}-r} dE \rho(E), \quad (11)$$

where  $\rho(E)$  is the density of states of the quasiparticle band with dispersion  $\epsilon(\mathbf{k})$ . The initial value of  $u(x, t = 0)$  is given by  $u^b(x)$  in (9). It is singular because of the delta-functions which is inconvenient for numerical solution of (10). Fortunately,  $p(t) = 1$  in the range  $0 \leq t \leq t_0$ , where

$$t_0 = \min G(\mathbf{k}) = 1/(r + E_{max}) = 1/(r + 2qK), \quad (12)$$

(see figure 1) and  $E_{max} = \max_{\mathbf{k}} \epsilon(\mathbf{k})$  is the upper edge of spectrum  $\rho(E)$ . It is easy to see that when  $p$  is constant, Eq. (10) turns into a linear diffusion equation for  $\exp[-u(x, t)]$ . The equation is solved exactly with the use of the Gaussian diffusion kernel [21, 15, 22] and at  $t = t_0$  the solution reads

$$\begin{aligned} e^{-u(x, t_0)} &= (2\pi t_0)^{-1/2} \int dx' e^{-(x-x')^2/2t_0} e^{-u^b(x')} \\ &= C e^{-x^2/2t_0} \left( 1 + 2e^{-(\Delta+qK/2)} \cosh \frac{x}{t_0} \right) \end{aligned} \quad (13)$$

where  $C = \det(\hat{G}/t_0)^{1/2N}$ .

The partition function (6) for homogeneous field  $h$  or, equivalently, the dimensionless FE per site is expressed in terms of the local potential in the LPA as

$$f(h) = -\ln Z(h)/N \simeq [u^R(x) - rx^2/2]_{x=h/r}. \quad (14)$$

Here and throughout the paper superscript “ $R$ ” will mean that the quantity is fully renormalized. In the case of the RG solution this will mean that its “time” coordinate  $t = t^R = 1/r$  is at the endpoint of the RG trajectory (see figure 1).

The accuracy of (10) can be improved by an appropriate choice of the arbitrary parameter  $r$ . In [15, 22] it was shown that good results can be obtained with the self-consistency (SC) condition consisting in the choice of  $r$  in such a way that it approximated the exact mass operator of the model in the long-wavelength limit

$$G^R(\mathbf{k} \rightarrow \mathbf{0}) \approx G(\mathbf{k} \rightarrow \mathbf{0}) = 1/r. \quad (15)$$

In terms of the local potential the condition reads [15, 22]

$$u_{xx}^R|_{h=0} = 0. \quad (16)$$

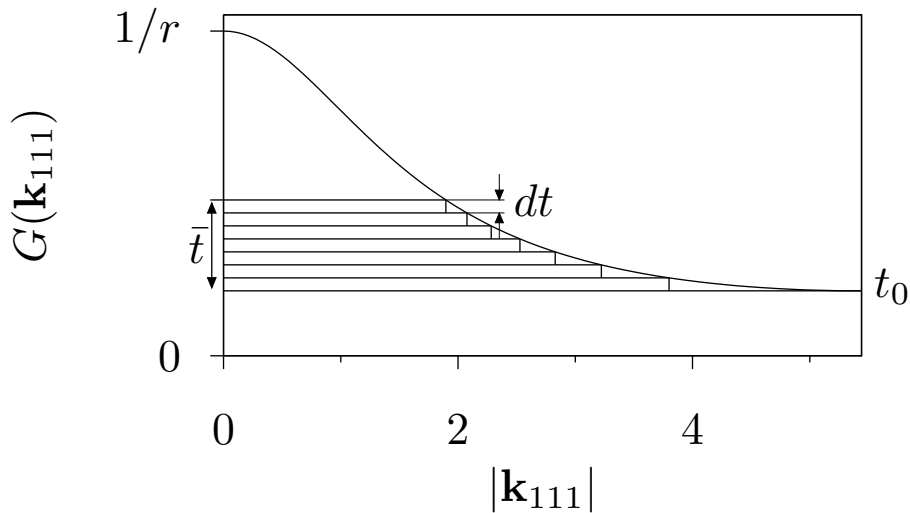


**Figure 1.** Illustration of the layer-cake renormalization scheme. The layers are cross-sections of  $dG = \theta[G(\mathbf{k}) - t]dt$  along the diagonal of the Brillouin zone on which  $G(\mathbf{k})$  reaches its minimum value  $t_0 = 1/(2qK + r)$ ;  $\bar{t} = t - t_0$ .

In this equation the external field is supposed to be equal to zero because in the present paper mainly this case will be of interest. However, in the BCM the phase transitions below  $T_{tr}$  occur also at the “wings” [32] at  $h \neq 0$ . In this case condition (16) should be correspondingly modified.

As explained in [15, 22] and will be further discussed in section 4 below, in the coexistence region (10) produces singular solutions difficult to deal with numerically. To overcome the problem, auxiliary local field variable  $y$  and auxiliary local potential  $v(y, t)$  were introduced via a Legendre-like transform

$$x = y + \bar{t}v_y \quad (17)$$

$$u = v + \bar{t}v_y^2/2 \quad (18)$$

where  $\bar{t} = t - t_0$ . In these variables (10) takes the form

$$v_t = \frac{p(t)v_{yy}}{2(1 + \bar{t}v_{yy})}, \quad (19)$$

and the evolution parameter varies from  $t_0$  to  $t^R = 1/r$ . The initial condition at  $t = t_0$  is obtained from (13)

$$v_0(y) = \frac{y^2}{2t_0} - \ln \left( 1 + 2e^{-(\Delta+3K)} \cosh \frac{y}{t_0} \right) - \frac{1}{2} \left( \frac{1}{N} \sum_{\mathbf{k}} \ln G(\mathbf{k}) - \ln t_0 \right) \quad (20)$$

with the use of the fact that at  $t = t_0$   $\bar{t} = 0$  so in (17) and (18)  $x = y$  and  $u(x, t_0) = v(y, t_0) = v_0(y)$ . The SC condition formally remains as in (16) [15, 22]

$$v_{yy}^R|_{h=0} = 0. \quad (21)$$

The physical field and the local potential are obtained from the auxiliary quantities (17) and (18) in parametric form as [15]

$$x = h/r = y + \bar{t}^R v_y^R \quad (22)$$

$$u^R = v^R + \bar{t}^R (v_y^R)^2 / 2 \quad (23)$$

Equations (19)—(21) will be called the SC-LPA RG equations. They will be solved numerically throughout the paper by numerical procedure described in [15, 22].

### 3. Continuous transitions in BCM

As was pointed out in Introduction, continuous phase transitions in BCM are located on three lines terminating at TCP. However, two of them bound the side “wings” appearing at  $h \neq 0$  (see figure 1 in [4]) while in the present paper we will restrict consideration mainly to case  $h = 0$  which was thoroughly investigated within MC and TSE methods [33, 30, 34, 35, 4] and our aim in the present paper is to validate present theory via its quantitative comparison with the most reliable alternative approaches.

At  $h = 0$  the critical line extends from  $D = -\infty$  where BCM coincides with the spin-1/2 Ising model to  $D_{tr}$  corresponding to TCP, as shown in figure 2. The critical temperature  $T_c$  at each  $D$  has been found as the temperature at which the SC value of  $r$  turned to zero (for details see [15, 22]). As can be seen,  $T_c$  predicted by the SC-LPA RG equation are in good agreement with the results obtained in numerical simulations and in TSE. Quantitatively the agreement can be characterized by comparison with six precision values of  $T_c$  presented in Table VI of [34] and with  $T_c$  for  $D = 0$  from [35]. The discrepancy varied in the narrow range in 0.02%–0.6% and taking into account that at  $D = -2$  in figure 2  $T_c \simeq 3.61$ , that is, in the interval  $-\infty < D < -2$   $T_c$  changes less than on 30% and that at the interval ends the SC-LPA predictions are off not more than on 0.6%, it seems plausible that this accuracy would hold for all values of  $D$  for the continuous transitions at  $h = 0$ .

#### 3.1. TCP

As mentioned in the introduction and discussed in detail in [36], TCP is the point of intersection of three critical lines and of one FOPT line. It means that, on the one hand, the behaviour of thermodynamic quantities in the vicinity of TCP is very complex but, on the other hand, there should be many ways of determining its position on the phase diagram. For example, when moving along a critical line the critical exponents will undergo an abrupt change at TCP from their Ising values (in the BCM case) to the TCP values. In particular, the exponent  $\eta$  jumps from  $\eta \approx 0.04$  [37] to  $\eta_{tr} = 0$  [23]. With the exception of  $\eta_{LPA}$  which is also zero, other LPA exponents undergo the jump because they differ from their TCP counterparts. Thus, TCP can be found as the point at the  $h = 0$  critical line where  $\gamma$  jumps from  $\gamma_{LPA} \simeq 1.3$  to  $\gamma_{tr} = 1$  and/or where  $\beta$  change its value from  $\simeq 0.325$  to 0.25.

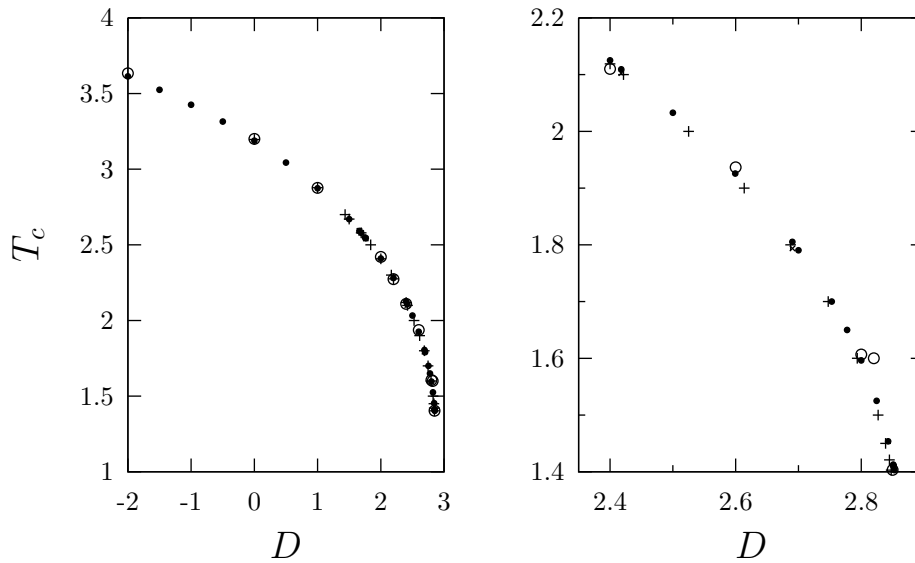


**Figure 2.** Comparison of the critical temperature of continuous phase transitions in the BCM calculated for different values of the anisotropy  $D$  by different techniques:  $\bullet$ —present study;  $\circ$ —numerical simulations of [30];  $\times$ —Monte Carlo simulations of [34];  $+$ —high temperature expansions of [4]. The lowermost points correspond to TCP (somewhat different in different approaches).

However, similar to other numerical studies [30, 4], in the SC-LPA it was difficult to obtain the truly abrupt change in the exponent values due to finite accuracy of the calculations. The cause of the problem was that on approach to TCP the critical region of the Ising universality class shrinks to zero, as can be shown analytically, e.g., in the mean field approximation [4] which is qualitatively correct for 3d TCP. So due to the limited accuracy of the computations, the critical behaviour on approach to TCP was not possible to study at distances smaller than  $\tau \lesssim 4 \cdot 10^{-3}$ . Within this distance the critical exponents have been fitted to the numerical data with the use of effective exponents [15] which exhibited a transient behaviour by changing from the LPA to TCP values. Fortunately, the interval of such behaviour was sufficiently narrow, in particular, it was much narrower than in TSE approach in [4], so the TCP coordinates in figure 2 determined in this way

$$D_{tr} = 2.853 \text{ and } T_{tr} = 1.403 \quad (24)$$

compare well with known estimates. For example, they differ only on less than 0.1% from the values found in MC simulations in [33] which in [4] were reckoned to be the most accurate among available to date.

An important advantage of the RG approach is that in contrast to MC and TSE techniques that rely solely on their numerical accuracy, the tricritical behaviour of the LPA RG equation can be analyzed analytically. Because the LPA equation (10) has been derived from the RG equation in [21], the linearized form of the latter can be used to determine the TCP critical exponents in the LPA. According to [23], at the TCP fixed point the local potential in 3d (the upper critical dimension) is equal to zero so



in the RG equation (12) of [21] linearized around the fixed point we should set (in the notation of that reference)  $d = 3$   $z^* = 0$  (hence,  $r = 0$ ),  $\beta = (d - 2)/8 = 1/8$  and  $n = 1$  (the Ising universality class) to get the equation defining the eigenfunctions  $e_j$  and the eigenvalues  $Y_j$  of the perturbations near the TCP fixed point:

$$-e_j'' + \left(\frac{x^2}{16} - 3\frac{1}{4}\right)e_j = -Y_j e_j. \quad (25)$$

With the use of operators  $a^\pm = 8^{-1/2}x \pm 2^{1/2}d/dx$  the equation can be cast in the form

$$\frac{1}{2}\hat{n}e_j = (3 - Y_j)e_j, \quad (26)$$

where  $\hat{n} = a^+a^-$  is the occupation number operator with the eigenvalues  $0, 1, 2, \dots$  which can be used as the index  $j$ . Thus,

$$Y_j = 3 - j/2 \quad (27)$$

in accordance with known exact values [23, 38, 39]. As is seen, the large eigenvalues that define the tricritical behaviour are those with smaller  $j$ . The first three of them are  $Y_0 = 3$ ,  $Y_1 = 5/2$  and  $Y_2 = 2$ . The largest eigenvalue  $Y_0$  simply reflects the fact that in 3d the FE of the system grows as the third power of the linear size. The non-trivial eigenvalues define the critical exponent  $\nu_{tr} = 1/Y_2 = 0.5$  and  $\beta_{tr} = (3 - Y_1)/Y_2 = 0.25$  [40, 41]. Now using the scaling relation  $\gamma = \nu(2 - \eta)$  (valid also at TCP [23]) with  $\eta_{tr} = 0$  one gets  $\gamma_{tr} = 1$  in complete agreement with the known exact values.

Determining TCP coordinates (24) through the jump in the critical exponents is, arguably, the most difficult way to proceed. An easier way would be to determine them by finding such  $D_{tr}$  that for  $D > D_{tr}$  the critical points with  $h, r = 0$  disappear. Several more methods exist in the FOPTs region. (i) TCP can be found as the point defining the start of the FOPT transition line, that is, the point at which the quartic term in renormalized local potential changes its sign [28], that is, when  $u_{xxxx}^R = 0$ . (ii) Further, the difference of FOPTs from the continuous transitions is that the spontaneous magnetization  $m_0$  (the subscript is for  $h = 0$  condition) at  $T_c$  (we will keep this notation also for FOPT temperatures) is finite. So TCP can be found as the point where  $m_0$  turns to zero on approach to TCP from below  $T_{tr}$ . (iii) Yet another way of determining TCP can be based on the fact that the latent heat of FOPTs disappears at TCP. All these possibilities have been tested in calculations below and deviations from (24) have been found to be O(0.1%).

#### 4. FOPTs as the shock wave solutions of the RG equation

In continuous transitions the critical temperature can be found as the point of divergence of the correlation length which in our formalism means  $r = 0$ . Alternatively, it can be determined as the point where the order parameter  $m_0$  switches from zero to non-zero values.

At the FOPTs, however, both  $r$  and  $m_0$  remain finite so usually  $T_c$  is defined as the temperature at which the FE curves  $f_o(T)$  and  $f_d(T)$  calculated, respectively, in the

ordered and in the disordered phases intersect. This implicitly presumes that  $f_o$  and  $f_d$  can be continued inside another phase. However, as pointed out in [4], this approach is controversial because thermodynamic quantities at the FOPT point are singular, though a detailed structure of the singularities is unknown (see [42, 43] and references therein).

But in the BCM the FOPT line at  $h = 0$  is the intersection of two symmetric surfaces of FOPTs called wings on which  $h \neq 0$  which join at  $h = 0$  (see, e.g., figure 1 in [4]). This can be used to determine the line of FOPTs at  $h = 0$  as follows. Let us for definiteness consider the wing at positive  $h$ . At a fixed value of  $D_{tr} < D < 3$  and  $T$  such that  $T_c(h = 0) < T < T_{tr}$  ( $T_c(h = 0)$  is the FOPT temperature of interest) the line parametrized by  $h > 0$  at some point  $h_c$  will pierce the wing. In crossing the surface the order parameter will abruptly change its value from, say,  $m_a$  to  $m_b$  (or from  $-m_a$  to  $-m_b$  for negative  $h$ ). At the  $m(h)$  isotherm this will be seen as the vertical line connecting two endpoints with different  $m$  but the same  $h$ , as can be seen in figure 3. The equation of state describing the lines in the figure has been obtained in parametric form by using equation (35) from [15]

$$m = -df/dh = y - t_0 v_y^R \quad (28)$$

for magnetization and (48) for  $h$ . At  $T_c(h = 0)$  both  $h_c$  and  $m_a$  turn to zero, so any of these quantities may be used as the order parameter of the transition. Similar to

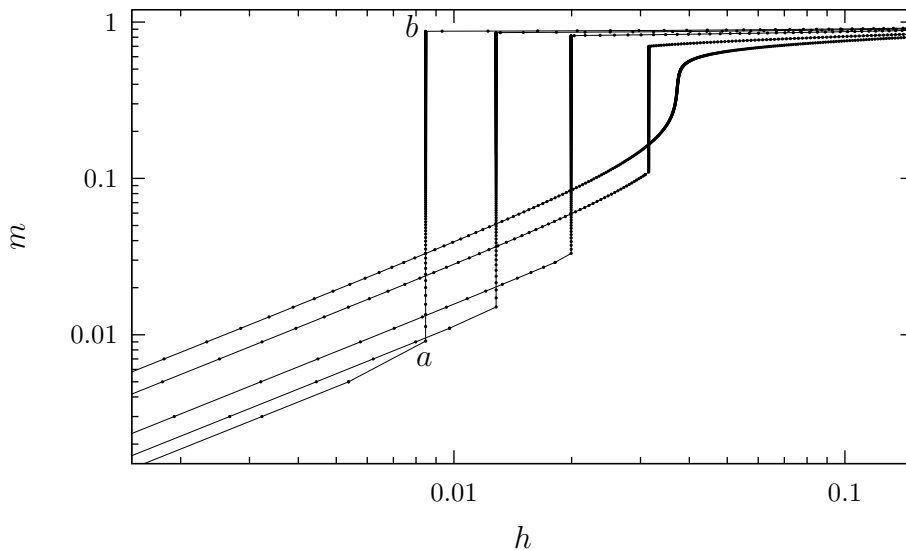


**Figure 3.** The equation of state ( $m(h)$  isotherms) in the wing region for  $D = 2.95$  and temperatures (from right to left)  $T = 1.27, 1.2, 1.1, 1.05$  and  $1.022$ . The calculated points are connected by lines for clarity. The rightmost curve corresponds to the temperature just above the wing critical temperature  $T_c^{(\text{wing})}$ .

the  $h = 0$  spin-1/2 Ising model studied in [15, 22], in BCM in the coexistence region at  $h = h_c \neq 0$  the auxiliary potential coincides with the particular Gaussian solution of (19) of the form

$$v_G(y, t) = -\frac{(y - h_c/r)^2}{2\bar{t}R} + (\text{f.i.t.}), \quad (29)$$

where (f.i.t.) denotes field-independent terms. Substitution of  $v_G$  into (17) shows that solution (29) corresponds to a constant external field  $h = h_c$ , that is, to the vertical lines in figure 3. Magnetization calculated from  $v_G$  with the use of (28) coincided within the accuracy of the calculations with  $m$  found from the numerical solution  $v^R(y)$  in the interval  $(y_a, y_b)$  corresponding to the interval  $(m_a, m_b)$ . This is analogous to the case of the spin-1/2 Ising model [15] where the Gaussian solution described the behaviour below  $T_c$  on the interval  $(-m_0, m_0)$ . This seemingly universal behaviour was first observed in solutions of an LPA RG equation in [9] and was tentatively attributed to a fixed point describing FOPTs. To clarify the issue in the present context it is instructive to switch from the auxiliary to the original variables  $x$  and  $u$ .

#### 4.1. LPA RG equation as generalized Burgers' equation

With the use of (14) magnetization can be found as

$$m(h) = \frac{h}{r} - \frac{u_x^R}{r} \Big|_{x=h/r}. \quad (30)$$

The first term on the r.h.s. describes the linear response to the external field while the second term may be called the non-linear response because due to the SC condition (16) this term contributes to  $m$  only in higher orders in  $h$ . Hence, the discontinuities in  $m(h)$  dependence may come only from this term. By differentiating (10) with respect to  $x$  it is easy to see that

$$\mu(x) = u_x(x) \quad (31)$$

satisfies the generalized Burgers' equation [27]

$$\mu_t + \mu\mu_x = (p/2)\mu_{xx} \quad (32)$$

which coincides with the conventional viscous Burgers' equation (BE) [44] when the "viscosity"  $p/2$  is constant. But in our case  $p$  is a function of "time"  $t$  and in [27]  $p(t)$  was interpreted as the cross section of a duct. Despite being dependent on  $t$ ,  $p(t)$  is positive so can play the role of the diffusion term and reproduce qualitatively the behaviour of the BE solutions. Furthermore, because  $p(t = t^R) = 0$ , it may be expected that fully renormalized  $\mu^R$  would behave similar to the inviscid BE in the zero-viscosity limit, in particular, exhibit the discontinuities seen in figure 3. This possibility will be discussed in more detail in section 4.3.

The RG equation in auxiliary variables for  $\mu(y, t) = v_y(y, t) = \mu(x, t)$ , where the last equality follows from equation (B.3) in [15]

$$u_x = v_y, \quad (33)$$

is straightforwardly derived from (19) as

$$\mu_t = \frac{p(t)\mu_{yy}}{2(1 + \bar{t}\mu_y)^2}, \quad (34)$$

In principle, (10) could be replaced by (32) without loss of generality because local potential  $u$  needed in the expression for FE (14) could be obtained by simple integration

of  $\mu$  from, say, 0 to  $x$ . The integration constant could be recovered from (13) augmented by integration over  $t$  of (10) at  $x = 0$  as

$$\Delta u^R(0) = \frac{1}{2} \int_{t_0}^{t^R} dt [p(t)\mu_x(0, t) - \mu^2(0, t)]. \quad (35)$$

However, (34) implicitly contains the third derivative  $v_{yyy}$  which in view of the discontinuous second derivative would introduce delta-function singularities into the equation causing difficulties in numerical solution. Besides, the derivation of GBE (32) by simply taking the derivative over  $x$  of (10) would not work for Landau-Ginzburg models with multicomponent vectors ( $n > 1$ ). The SC-LPA RG equations for such models derived in [22] directly generalize (10) to  $n$ -component case. When  $p = 0$  they acquire the form of the Hamilton-Jacobi equations and in this form also can be used for the description of FOPTs [45, 46]. Therefore, all numerical calculations in this paper have been done with the use of equations for  $u$  and  $v$ . BE in different forms have been used only to clarify the shock wave features of the solutions because it is a conventional framework for such analysis [44, 47, 48, 45].

#### 4.2. Infinite range Ising model

To gain qualitative insight into (32), let us apply it to a simple case where most calculations can be performed analytically. The infinite-range Ising model (IRIM) also known as the Husimi-Temperley [48] and the Curie-Weiss model [49] can be solved exactly within the MF theory for all values of the model parameters with the exception of the coexistence region where the unphysical van der Waals loops appear. In [48, 45] it was shown how they can be avoided with the use of BE in the solution of the model. Incidentally, IRIM can be also solved exactly within the SC-LPA RG approach. Therefore, below we will show how equation (32) can be used in the solution of the problem of the van der Waals loops within the RG approach.

Similar to the Landau MF theory [28], IRIM is a structureless model because when a spin interacts with the same strength with any other spin in the system it does not matter how far apart the spins are, what is the lattice they are on or whether it at all exists. Therefore, in matrix  $\hat{\epsilon}$  in (3) we do not specify the topology but formally set the coordination number  $q = N - 1$  and define interactions between spins at different sites to be  $J/N$  where  $J = O(1)$ . From the requirement  $\sum_j \hat{\epsilon}_{ij} = 0$  equivalent to (4) on any lattice it is easy to find

$$\hat{\epsilon}^\infty = K(\hat{I} - \hat{E}) \quad (36)$$

where  $K = J/T$  is formally the same as in (3),  $\hat{I}$  is the unit matrix and in matrix  $\hat{E}$  all matrix elements are equal to  $1/N$ . Matrix  $\hat{E}$  is idempotent ( $\hat{E}^2 = \hat{E}$ ) and so such is  $\hat{I} - \hat{E}$ . The spectrum of idempotent matrices consists of only two points: 0 and 1, so the two values of the spectrum of  $\hat{\epsilon}^\infty$  are 0 and  $K$ . The corresponding density of states can be found as  $\rho(E) = \Im G_{ii}(E + i\varepsilon)/\pi$ . So using easily derivable expression

$$-\left(\frac{1}{z - \hat{\epsilon}^\infty}\right)_{ii} = -\frac{1}{N} \frac{1}{z} - \left(1 - \frac{1}{N}\right) \frac{1}{z - K} \quad (37)$$

with  $z = E + i\varepsilon$  (the minus signs before all terms have been introduced for compatibility with (5)), one gets

$$\rho^\infty(E) = N^{-1}\delta(E) + \delta(E - K) \quad (38)$$

where in the second term  $1/N \ll 1$  have been neglected. The upper edge of the spectrum  $E_{max} = K$  fixes the lowest value of the evolution parameter  $t$  defined in (12) as

$$t_0^\infty = 1/(r + K) \quad (39)$$

The upper integration limit corresponds to  $\max G = 1/(r + E_{min})$  (see figure 1) with  $E_{min}$  always equal to zero in the present formalism. Thus, the total density of states needed in (11) is

$$\rho_{tot}^\infty(E) = N^{-1} + \theta(E - K). \quad (40)$$

Using (11) and (40) it is easy to see that in the whole integration range  $t^R < t < t_0^\infty$

$$p^\infty(t) = \rho_{tot}^\infty(t^{-1} - r) = N^{-1}. \quad (41)$$

Thus, GBE (32) in this case takes the form of the conventional BE with constant viscosity  $1/2N$

$$\mu_t^\infty + \mu^\infty \mu_x^\infty = (1/2N)\mu_{xx}^\infty \quad (42)$$

and coincides with equation (3.2) derived in [48] in a different approach. Now following that paper we could linearize BE with the use of the Cole-Hopf substitution and analyze the solution along the lines of [48]. However, our aim is not to solve IRIM by the RG technique but to show that the method of solution of GBE (32) used in this paper and [22, 15] leads to the shock wave solutions at FOPTs similar to those suggested in [48, 45] for IRIM.

To begin with, let us discuss, how the mechanism by which even an infinitesimal viscosity in BE suppresses the multivalued solutions of inviscid BE, can be understood in the framework of the SC-LPA RG approach. To this end, let us first discard the viscosity in (42) by taking the naive thermodynamic limit  $N \rightarrow \infty$  to obtain the inviscid BE. Now the corresponding equation (34) in the auxiliary variables in the IRIM case reads

$$\mu_t^\infty(y, t) = 0. \quad (43)$$

With the parameters corresponding to  $\hat{\epsilon}^\infty$  the initial condition for the spin-1/2 Ising model given in equation (A.14) of [15] reads

$$u_0^\infty(x) = \frac{x^2}{2t_0^\infty} - \ln \left( 2 \cosh \frac{x}{t_0^\infty} \right). \quad (44)$$

Differentiation with respect to  $x$  gives the initial condition at  $t = t_0^\infty$  for (42) as

$$\mu_0^\infty(x) = [x - \tanh(x/t_0^\infty)]/t_0^\infty. \quad (45)$$

The initial  $\mu_0^\infty(y)$  can be obtained from (45) by simply replacing  $x$  in (45) with  $y$  because as already mentioned, according to (17) and (18) the variables coincide at

$t = t_0$ . Further, because according to (43)  $\mu^\infty(y)$  does not depend on  $t$ , we immediately obtain the solution in auxiliary variables

$$\mu^\infty(y) = [y - \tanh(y/t_0^\infty)]/t_0^\infty \quad (46)$$

and similarly for the local potential

$$v^\infty(y) = \frac{y^2}{2t_0^\infty} - \ln \left( 2 \cosh \frac{y}{t_0^\infty} \right) \quad (47)$$

(cf. with (44)). The subscripts 0 have been omitted in the last two expressions because the solutions are valid at all  $t$ , in particular, at  $t = t^R$  which will be implicitly assumed everywhere below unless stated otherwise.

As noted previously, due to (33)  $\mu(x, t) = \mu(y, t)$  so to determine  $\mu^\infty(x, t^R)$  (46) should be augmented by (22) which defines the dependence of  $x$  on  $y$

$$x = h/r = y + \bar{t}^R \mu^R. \quad (48)$$

With the use of (39) and (46) (48) can be conveniently written as

$$h = y/t_0^\infty - K \tanh(y/t_0^\infty). \quad (49)$$

. Another measurable quantity—magnetization—is given by (28) which in terms of  $\mu$  reads

$$m = y - t_0 \mu^R. \quad (50)$$

Substitution here of (45) gives

$$m = \tanh(y/t_0^\infty). \quad (51)$$

In conjunction with (49) it leads to the exact IRIM MF equation [49]

$$m = \tanh(Km + h) \quad (52)$$

for determining the equilibrium magnetization in terms of temperature and the external field. In particular, from (52) it is easy to find that when  $h = 0$  the critical temperature  $T_c = 1$ , as follows from  $1/T_c = K_c = 1$ . Besides, by comparing the last two equations it is easy to see that the spontaneous magnetization  $m_0$  and corresponding to it  $y_0$  in figure 4 are proportional to each other

$$m_0 = y_0/Kt_0. \quad (53)$$

Finally, expressing  $u^R$  in (23) through (47) and  $\mu^R = v_y^R$  and substituting this into FE (14), where the last term with the use of (48) should be expressed through  $y$  and  $\mu^R$ , one obtains an expression for FE in terms of  $y$  and  $\mu^R$ . Now noting that the argument of the hyperbolic cosine is the same as in (52) and rearranging remaining terms so as to express them through  $m$  from (50) one arrives at the exact expression for IRIM FE [49, 48]

$$f^\infty = Km^2/2 - \ln [2 \cosh(Km + h)]. \quad (54)$$

The obtained solution of IRIM is exact everywhere except in the coexistence region where it exhibits the unphysical van der Waals loops characteristic of MF theories. In

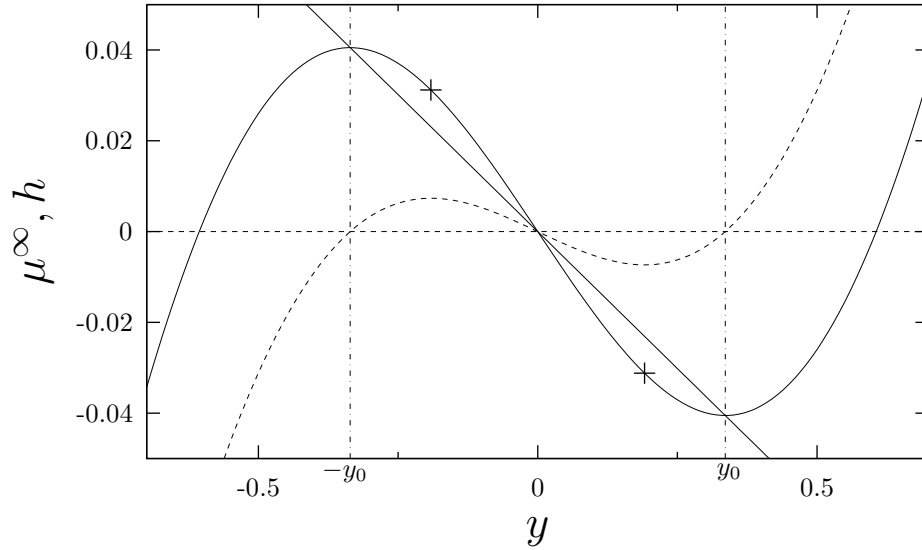


**Figure 4.** Plots of  $\mu^\infty(y)$  (46) (solid curve) and  $h(y)$  from (49) (dashed curve) that define  $\mu^\infty(h)$  for IRIM in parametric form at  $K = 1.05$ . Straight solid line is  $\mu_G$  (57); dashed-dotted lines bound the coexistence region,  $y_0$  is from (53); symbols (+) bound the segment of  $\mu^\infty$  curve where it is steeper than  $\mu_G$ .

terms of  $\mu^\infty(x, t)$  this can be seen from the graphs of  $h(y)$  and  $\mu(y)$  shown in figure 4. For any value of  $h$  in the range between the two local extrema there are three values of  $y$ , hence, three values of  $\mu^\infty(y)$ . So  $\mu^\infty(h)$  is a three-valued function in this range.

To see how the viscosity, even infinitesimal, can resolve the problem of the van der Waals loops let us consider equation (34) as a diffusion equation with the diffusivity depending on spatiotemporal coordinates:

$$\mathcal{D}(y, t) = \frac{p(t)}{2(1 + \bar{t}\mu_y)^2} \quad (55)$$

In the discussion below we will often omit references to IRIM because the majority of arguments are expected to be valid in general case. The qualitative picture presented below have been observed in the numerical solutions of the SC-LPA RG equations for BCM and the Ising model.

Because we will be interested in the behaviour of the diffusivity in the coexistence region where derivative  $\mu_y$  is negative, to simplify the discussion let us introduce the minus sign explicitly into the expression in the parentheses in the denominator of (55) as

$$\Psi(y, \tau) = 1 - \tau|\tilde{\mu}_y| \quad (56)$$

where additionally the normalized quantities  $\tau = \bar{t}/\bar{t}^R$  and  $\tilde{\mu} = \bar{t}^R\mu$  have been introduced. Their convenience is that during the evolution  $\tau$  varies from 0 to 1 so from (56) it is obvious that  $|\tilde{\mu}_y^R|$  cannot exceed unity because in this case  $\Psi^R$  would be negative which means that at some  $\tau_c > 0$  it crossed zero because  $\Psi(y, 0) = 1 > 0$ . But if  $p \neq 0$  this would introduce in  $\mathcal{D}$  nonintegrable singularity in  $t$  which means that the renormalization would not be possible to complete. In fact, on approach to  $\tau_c$  the

diffusivity will acquire arbitrarily large values even for smallest viscosity. The enhanced diffusion will be smearing  $\mu(y, t)$  until making the slope  $|\tilde{\mu}_y|$  smaller than unity.

Thus, the steepest  $y$ -dependence of  $\mu^R$  compatible with viscosity is  $-1/\bar{t}^R$  which coincides with the slope of  $\mu^R$  corresponding to the Gaussian solution (29). It has always been obtained in the coexistence region in BCM and Ising models in the numerical solutions of (19). The linear function

$$\mu_G(y) = -\frac{y - h_c/r}{\bar{t}^R} \quad (57)$$

for the symmetric case  $h_c = 0$  is drawn in figure 4. Comparison with  $t$ -independent solution of IRIM (46) shows that the latter cannot be valid at all  $t$  because in the segment between the crosses  $\mu^\infty$  is steeper than  $\mu_G$ . Thus, with the inclusion of viscosity at least this segment will be flattened by diffusion in the course of evolution, thus making  $\mu^\infty$  dependent on  $t$ . In the case of IRIM it is easy to show that at the end of evolution the initial  $\mu^\infty(y)$  curve within the segment in figure 4 will coincide with  $\mu_G$ . The evolution toward  $\mu_G$  of the parts of the curve outside the segment is not straightforwardly seen from the form of diffusivity (55). So instead the numerical procedure that has been used in the solution of BCM has been applied to (19) for IRIM with  $N = 10^3$ . The Gaussian potential (29) corresponding to the thermodynamic limit  $N \rightarrow \infty$  has been obtained for  $h_c = 0$  in the whole coexistence region with the accuracy better than 0.01%. When substituted in (48) it gives  $h = 0$  within the region which means that when  $h$  crosses zero, the magnetization jumps from, say,  $m_0$  to  $-m_0$ , as expected. Thus, the RG flows during FOPTs in BCM and in the Ising model are qualitatively the same as in the exactly solvable and well understood IRIM [48, 45].

### 4.3. FOPT fixed point

The qualitative behaviour just described suggests that the RG trajectory inside the coexistence region terminates with a universal function (29) which potentially is a candidate for the discontinuity fixed point advocated in some approaches [50, 42, 20, 43, 9]. The attraction basin of the point consists of Hamiltonians with initially renormalized  $\mu_0(y)$  having regions of  $y$ -dependence with negative slope exceeding that of  $\mu_G$  or, equivalently, with the negative curvature of  $v_0(y)$  larger in absolute value than the curvature of  $v_G$ . The universal behaviour, however, does not comprise the whole range of variation of the local field  $y$ , as in continuous transitions. In BCM in the fully renormalized case it is restricted to finite intervals in the auxiliary variables  $(y_a, y_b)$ , where  $y_{a(b)}$  correspond to magnetizations  $m_{a(b)}$ , in the wing region at  $h_c \neq 0$  (see figure 3) or to  $\pm m_0$  in the zero field case. This apparently is a consequence of the finite amplitude of fluctuations of the order parameter in FOPTs. In physical variables in the fully renormalized case this range even shrinks to one discontinuity point:  $x_c = h_c/r$ .

Discontinuities are crucial for the description of FOPTs so to get physical insight into the RG flow leading to them in physical terms let us approximate  $\mu(x, t)$  for  $t \rightarrow t^R$  as follows. First, let us assume that in the coexistence region and for  $t$  close to  $t^R$



$\mu(y, t) \approx \mu_G(y)$ . Using  $\mu(y, t) = v_y = u_x = \mu(x, t)$  and replacing in (17)  $v_y$  by  $\mu(x, t)$  one finds that  $y = x - \bar{t}\mu(x, t)$ . Substituting this into the r.h.s. of (57) and replacing on the l.h.s.  $\mu_G(y)$  by  $\mu(x, t)$  one finds

$$\mu(x, t) \approx -\frac{x - x_c}{t^R - t} \equiv \frac{\Delta x}{\Delta t}. \quad (58)$$

As is seen, in the coordinates relative to the ‘‘critical point’’  $(x_c, t^R)$  the function is universal being independent of all parameters of the system under consideration. Also, when  $\Delta t \rightarrow 0$  the slope of  $x$ -dependence tends to infinity, as is necessary for the susceptibility in the coexistence region to be infinite. The range of validity of (58), i.e., the coexistence region in physical coordinates, can be easily assessed in the symmetric case  $x_c = 0$  using the fact that as  $t \rightarrow t^R$  and  $|h|$  is small, according to (30)  $\mu(x, t) \approx -rm_0 \text{sgn}(x)$  ( $m_0 > 0$ ). But because  $\mu(x, t)$  is a derivative of a smooth function  $u(x, t)$  it should be continuous so for small  $x$  and  $t \rightarrow t^R$  it can be modelled by a smeared sign function as

$$\mu(x, t) \approx \begin{cases} -rm_0 \text{sgn}(x) & |x| \geq x_0 \\ \mu_G(x, t)|_{x_c=0} & |x| < x_0 \end{cases} \quad (59)$$

where  $x_0 = rm_0(t^R - t)$ . As can be seen, the universal fixed point in the fully renormalized case  $t = t^R$  reduces to the jump in  $\mu^R(x) \simeq -rm_0 \text{sgn}(x)$  at a single point which simply corresponds to switch of magnetization from  $-m_0$  to  $m_0$  when the external field  $h$  crosses zero (or from  $m_a$  to  $m_b$  when  $h$  crosses  $h_c$ , as in figure 3). The singular part of FE acquires the form  $f_{sing} \simeq m_0|h|$  which is easily guessed on phenomenological grounds [50, 20]. From the RG standpoint, however, the result is not trivial because the singularity in  $u^R$  has been obtained by renormalization of the Landau-Ginzburg Hamiltonian which by definition is analytic in the fluctuating field (see (13)).

Thus, to adequately describe FOPTs it seems sufficient to have  $\mu^R(y, t) = \mu_G(y)$ , or, equivalently,  $v = v_G$  inside the coexistence region. However, there is a caveat. From mathematical literature [44, 47] it is known that infinitely steep shock waves may occur only in the inviscid BE and thus are incompatible with viscosity. In physical terms this can be seen by substituting (58) in (35). Because of the nonintegrable singularity, the contribution to  $u$ , hence, to FE through (14), diverges while FE should be finite and  $O(1)$ . In the IRIM case  $p = 1/2N$  so in order the integral of the first term in (35) was finite and  $O(1)$  the derivative  $\mu_x^R(0, t^R)$  should be  $O(N)$ , as indeed was found in [48]. But this is incompatible with (58).

In IRIM the necessary discontinuity is recovered in the thermodynamic limit  $N \rightarrow \infty$  but in short-range models  $p(t)$  is nonzero for all  $t$  except at  $t = t^R$  where the integration range in (11) shrinks to zero. This would be enough to make the integral in (35) convergent but may be insufficient for the appearance of the sharp shock waves in GBE (32). In such waves we expect  $\mu(x, t)$  to acquire the form of  $\mu(x, t)$  in (58). But when substituted in (32) the denominator of  $\mu(x, t)$  will effectively differentiate  $p(t)$  at  $t^R$  so the r.h.s. of the RG equations will become effectively proportional to  $p'(t^R)$ . The latter is proportional to  $\rho(E = 0)$  which is zero in the nn models that we have been

dealing with, so (32) would approach the inviscid BE for such models at the end of the evolution. This observation have been checked by application of the SC-LPA RG equation to the solution of a test model with  $\rho(E) \neq 0$  and no transitions have been found. This fact may be the cause of the poor performance of LPA in 2d case. The problem may disappear if momentum-dependent corrections to  $r$  would make  $\rho(E = 0)$  equal to zero. This, however, will require going beyond LPA.

## 5. FOPTs in zero external field

In previous section the regions of the phase diagram in the wings that appear in BCM below  $T_{tr}$  have been briefly discussed. Their detailed description in the MF approximation can be found in many papers [6, 32, 7, 4] but reliable MC or TSE data seems to be absent, so for the quantitative comparison we restrict our consideration to much better studied zero-field case [29, 33, 30, 34, 4].

Besides the vanishing of  $h_c$  and/or  $m_a$  suggested in previous section as the ways of determining  $T_c$  of the zero-field FOPTs in BCM, other methods can be used. As noted earlier, conventionally FOPTs are defined as the points where the values of free energies in two phases coincide, i.e., where  $f_d = f_o$ . The peculiarity of the numerical SC-LPA RG solutions was that they were unique in the sense that it has been impossible to continue the disordered solution below  $T_c$  and the ordered one above  $T_c$ . This suggests yet another way of determining the transition temperature as the point where the ordered solution disappears and the single coexistence region below  $T_c$  splits into two wing coexistence regions, as in figure 3. This method has appeared to be the most practical because the temperature step could be chosen sufficiently small to guarantee desired accuracy.  $T_c$  value has been placed at the middle point between the ordered solution at lower temperature and the disordered solution one step above.

In the present paper all above methods have been used in the determination of the transition temperatures shown in figure 5. At many points two or three of them have been compared and within the accuracy of calculations no discrepancies were found. Part of the results of [4] obtained via TSE are also shown in figure 5 for comparison. The authors pointed out that the FOPTs temperatures obtained from the condition of equality of the FE in the two phases seems to be systematically underestimated. They arrived at this conclusion by application of the method to the continuous transitions with  $T_c$  reliably determined by different technique (see figure 5). The RG points seems to correct this deficiency, in particular, because they linearly approach TCP which coordinates (24) have been determined with high accuracy. The linear slope was practically the same as above TCP (for the data shown in figure 2) which is the expected behaviour [4]. The transition temperature at the point taken from the numerical simulations of [30] seems to be too high to fall on the line passing through TCP with the same slope as in the continuous transitions range. Thus, it is quite plausible that the SC-LPA RG equation predicts FOPT temperatures in the BCM more accurately than the currently available TSE and the numerical simulation methods.

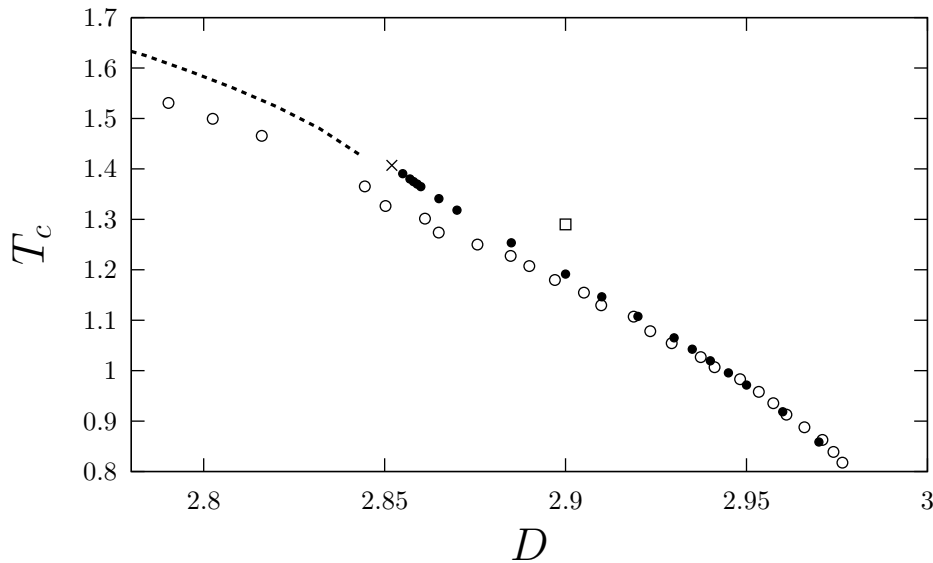


**Figure 5.** Zero-field FOPT temperatures (black points) and the TCP ( $\times$ ) at different values of anisotropy  $D \geq D_{tr}$  calculated within SC-LPA RG approach. For comparison are shown the FOPT and the continuous transition temperatures (open circles and the dashed line) calculated from TSE in [4]. The square is a FOPT temperature obtained in numerical simulations in [30]. For further explanation see the text.

### 5.1. Magnetization and the nonordering density at FOPTs

Below  $T_{tr}$  the spontaneous magnetization at FOPT temperature  $T_c$  is finite but approaches zero as  $T_c \rightarrow T_{tr}$ ;  $m_0(T_c)$  dependence calculated in the present approach is shown in figure 6. As is seen, the dependence can be roughly separated into a low-temperature region and a near-TCP region separated by a temperature interval with transient behaviour. In both regions similar power-law behaviour can be observed but with different amplitudes. Unfortunately, reliable independent data on  $m_0(T_c)$  are apparently absent in literature. Understanding this unusual behaviour would be important for the present study because the magnetization significantly influences the latent heat which will be calculated below in the near-TCP region. Of major concern in this respect is the power-law behaviour with exponent 0.25 near TCP which is very steep so the numerical solution of the RG equation with the use of a relatively large step ( $O(10^{-3})$ ) in  $y \propto m$  could introduce systematic errors into  $m_0$ . The step size was dictated by the software used in the calculations [22, 15] so to resolve the issue calculations within independent techniques and/or the use of better precision software [25] would be needed.

The non-ordering density [36] is equal to the concentration of sites with  $s_i = 0$ . It can be found by subtracting the ordering density, that is, the density of magnetic atoms with  $s_i = \pm 1$  from the total *per site* density which is equal to one

$$X = 1 - \langle s_i^2 \rangle = 1 - df/d\Delta \quad (60)$$

$$= 1 - m_0^2 - G_{ii}^R \quad (61)$$

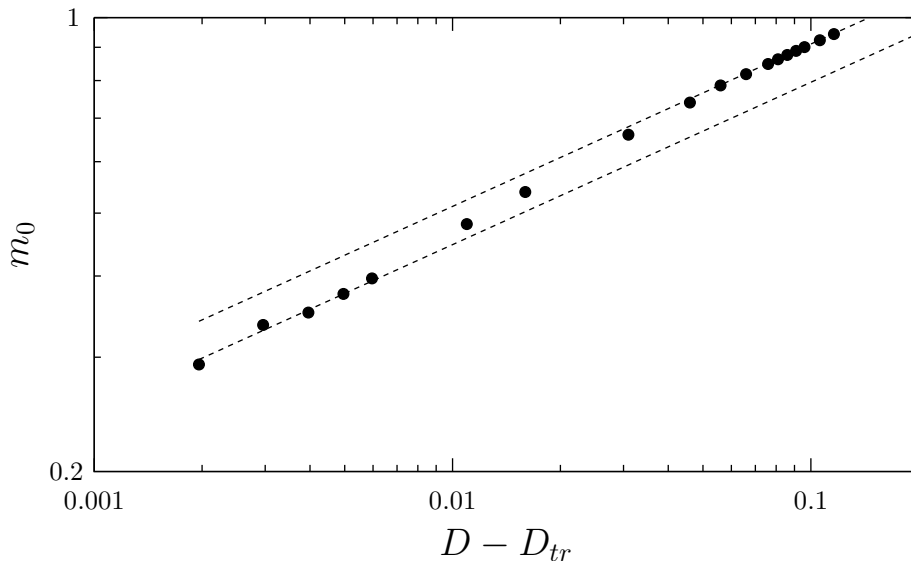


**Figure 6.** Symbols—dependence of spontaneous magnetization at FOPT on the distance to  $D_{tr}$  calculated in the SC-LPA RG approach; dashed lines—power-law dependence  $(D - D_{tr})^{1/4}$  fitted to the data in the two regions discussed in the text.

where site  $i$  can be chosen arbitrarily due to the homogeneity. Equation (60) follows from (14) differentiated by  $\Delta$  and (61) from (6) differentiated twice by  $h_i$ . Though equivalent in the exact theory, the two definitions have different status in the LPA because in (61) enters the fully renormalized correlation function  $G^R$  which is not calculated in the SC-LPA because this requires knowledge of the full momentum dependence of  $G^R(\mathbf{k})$  while in LPA according to (15) only  $k \rightarrow 0$  limit is available. Still, this approximation is not very bad as is illustrated by the dashed-dotted curve in figure 7.

But the best accuracy should be expected with the use of (60). The values calculated with the direct use of this equation above  $T_{tr}$  are shown in figure 7 by open circles. Their accuracy is confirmed by two facts. First, at TCP the calculated  $X_{tr}$  differs from the MC value of [33] by only 0.2% while the TSE value of [4] on almost 3%. Second, at the negative end of  $D$  values BCM becomes the Ising model. But introducing term  $\Delta s_i^2$  into the Ising model the initial local potential will acquire additional constant term— $\Delta$ —which will remain in the fully renormalized FE unaffected by renormalization because the LPA RG equations contain only derivatives. Thus, in the limit  $D \rightarrow -\infty$   $df/d\Delta = 1$ —the exact average value of  $s_i^2$  in the spin-1/2 Ising model.

In the FOPTs region below  $T_{tr}$  the direct application of (60) becomes more difficult because there are two branches on one of which the spontaneous magnetization have to be self-consistently determined which degrades the accuracy. This makes calculation of  $f$  at different  $D$  needed in (60) either less accurate or more computationally demanding if higher finite differences with larger number of points would be used. Therefore, for  $D$  close to the limiting value  $D = 3$  where the dependence on  $D$  becomes strong, the densities  $X_{d,o}$  have been calculated with the simpler (61) with  $G^R \approx G$  (see figure 7) while near TCP (60) was used indirectly as follows. To reduce the computational effort

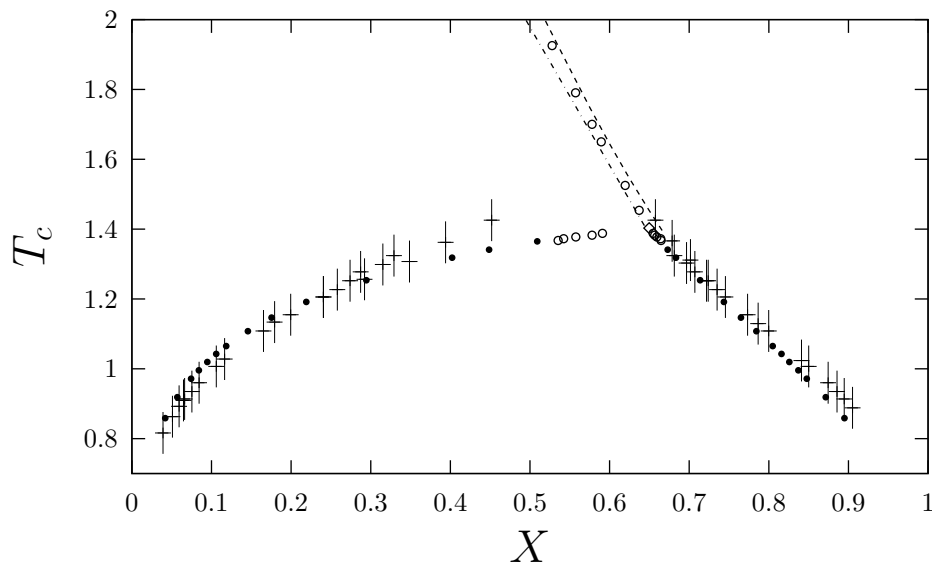


**Figure 7.** Dependence of the phase transition temperature on non-ordering density  $X = 1 - \langle s_i^2 \rangle$ . The dashed line and the crosses are the TSE data from [4]; the open circles and the diamond (at TCP) have been calculated within SC-LPA approach according to (60); the black dots and the dashed-dotted line have been calculated with the use of (61) with  $G^R$  approximated by  $G$ .

by using already calculated data, the derivative of  $f(T_c, D)$  over  $D$  along the FOPTs line which we denote by  $C$  has been calculated as

$$\left. \frac{df}{dD} \right|_C = \left. \frac{\partial f}{\partial T} \right|_{T=T_c} \frac{dT_c}{dD} + \frac{\partial f}{\partial D}. \quad (62)$$

In view of the definition  $\Delta = D/T$ , the last term on the r.h.s. of (62) can be used to write the non-ordering density in (60) as

$$X_{d,o} = 1 - T_c \left( \left. \frac{df}{dD} \right|_C - \left. \frac{\partial f_{d,o}}{\partial T} \right|_{T=T_c} \frac{dT_c}{dD} \right). \quad (63)$$

Because at  $T_c$   $f_o = f_d$ , among the terms on the r.h.s. of this expression only the temperature derivative is phase-dependent. Many such derivatives already have been calculated in the extrapolations needed to determine  $T_c$  from the condition  $f_o = f_d = f$  which automatically provided also the value of  $f(T_c, D)$ . Thus, only already known quantities can be used in (63). The derivatives over  $D$ , however, can be reliably calculated only when the values are sufficiently narrowly spaced. This was the case for several points closest to TCP where  $\Delta D = 10^{-3}$  has been used.  $X_{d,o}$  calculated in this way are shown in figure 7 below  $T_{tr}$  by open circles. Unfortunately, the TSE data are unavailable in this region but as can be seen the circles lie on the line interpolating the black points calculated via (60) toward TCP. The black points agree well with the TSE data farther from TCP but the agreement worsens on its approach. This divergence, however, is most probably due to inaccuracy of the TSE calculations because the TSE points closest to TCP have temperature coordinates larger than  $T_{tr}$  which is impossible because above the tricritical temperature the transitions should be continuous, not of

the first order. Thus, the RG calculations agree with the TSE farther from TCP, correct the unphysical behaviour of TSE on approach to TCP and, besides, can be carried out in the most interesting region in the vicinity of TCP.

### 5.2. The latent heat

Determination of the latent heat near TCP is one of the least studied problems in BCM because only one calculation by the MC technique seems to be available [29]. Part of the data [29] are shown in figure 8 together with the values calculated within the present approach. In the RG calculations the difference between the internal energies  $e$  [29] in the disordered ( $d$ ) and ordered ( $o$ ) phases

$$Q_{lat} = e_d - e_o \quad (64)$$

was found with the use of the Gibbs-Helmholtz equation that follows from (14) (with  $h = 0$ ) valid in both phases

$$e = -T^2 \partial f / \partial T. \quad (65)$$

In (64) and (65) use has been made of the temperature derivatives found in the linear interpolation of the free energies to determine  $T_c$ .

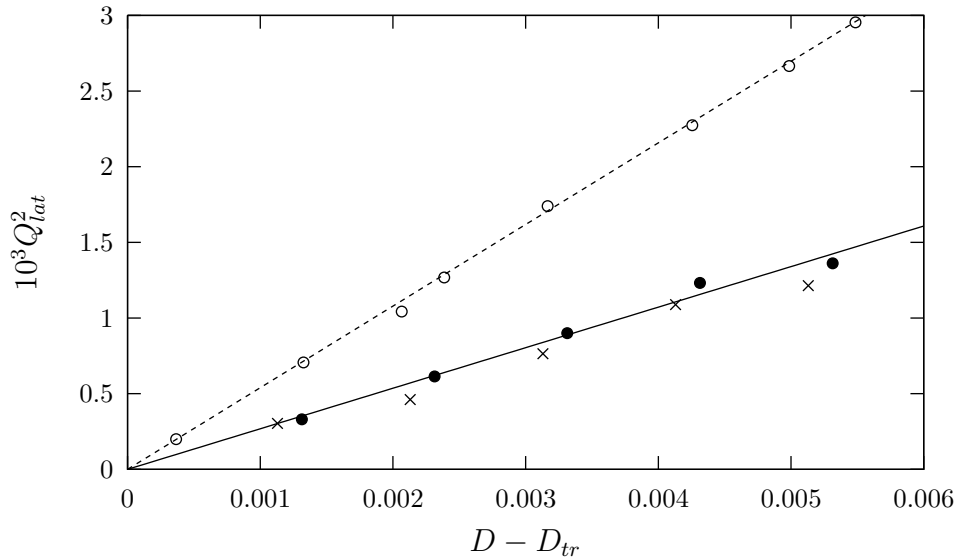


**Figure 8.** Latent heat for anisotropy  $D$  in the vicinity of TCP. Black points—calculations according to (64) within the present approach; open circles—the data taken from [29]. The lines are the best fits to the data. For comparison are shown the points calculated according to (66) ( $\times$ ).

As can be seen, the calculated absolute values of  $Q_{lat}$  disagree with MC data on about 40% in stark contrast with previous comparisons. However, to draw definite conclusions about the accuracy of any of the data shown in figure 8, additional studies would be necessary for the following reasons.

The data of [29] do not correspond to the thermodynamic limit but are calculated in a finite system with the linear box size  $L = 10$  lattice units. The interpolation to  $L = \infty$  was not attempted presumably because simulations with larger box sizes did not show the expected large- $L$  behaviour [29]. But there are reasons to believe that in the thermodynamic limit the absolute value of the latent heat will be essentially reduced. In the simulation of FOPTs in the 3-state Potts model on the sc lattice which is physically similar to BCM [51] it was found [52] that in the system with  $L = 32$  the latent heat is 12% smaller than in the system with  $L = 16$ . Assuming the leading correction to be due to the surface term, that is, assuming the latent heat at finite sizes to behave as  $Q_{lat}(1 + \delta/L)$  it is easy to find that at  $L = 10$  the heat will be  $\sim 40\%$  larger than  $Q_{lat}$ . But to confirm this estimate the interpolation within MC simulations of BCM or the TSE calculation would be necessary.

The SC-LPA RG calculation of  $Q_{lat}$  also is not devoid of difficulties. The problems arise because of the steep behaviour of the magnetization near TCP due to  $\beta = 0.25$  which necessitate the solution of additional self-consistency equation in the ordered phase [15, 22]. This is further aggravated by the fact that the quantity of interest ( $Q_{lat}$ ) vanishes at TCP so in its vicinity it is small but can be found only as a difference between two quantities ( $e_d$  and  $e_o$ ) that are finite at the transition. Thus, even their calculation with a good precision does not guarantee that the difference will be equally accurate.

A convincing test of the accuracy of the RG calculation of the latent heat could have been obtained from TSE simulations of [4] if the calculations of  $X(T)$  diagram below  $T_{tr}$  were continued closer to TCP to the region of the open circles in figure 7. In this case  $Q_{lat}$  could be expressed through the non-ordering density as follows. With the use of (64), (65) and (63) it is easy to derive expression for the latent heat in terms of  $X$  as

$$Q_{lat} = T_c \left| \frac{dT_c}{dD} \right|^{-1} (X_d - X_o). \quad (66)$$

In the vicinity of TCP  $T_c(D)$  dependence is approximately linear so the difference of  $X$  values in (66) behaves as [23, 4]

$$\Delta X \simeq A_1(T_{tr} - T_c)^{1/2} \simeq A_2(D - D_{tr})^{1/2} \quad (67)$$

where  $A_{1,2}$  are some constants. So the good agreement between  $\Delta X$  calculated by TSE and the RG (black points) seen on the phase diagram figure 7 could mean that closer to TCP (the open circles) the agreement would be similarly good and so TSE would confirm quantitatively the RG calculations of the latent heat. Unfortunately, the range of validity of (67) is unknown, except that it should hold asymptotically close to TCP. But from (61) one gets

$$\Delta X = m_0^2 + (G_{ii}^R)_o - (G_{ii}^R)_d. \quad (68)$$

It has been found that in the approximation  $G_{ii}^R \approx G_{ii}$  the last two terms on the r.h.s. practically cancel each other so  $\Delta X \approx m_0^2$ . As discussed earlier, it would be impossible

to fit  $m_0^2$  to the dependence (67) with the same constant  $A_2$  in the whole  $D - D_{tr}$  region shown in figure 6. Thus, unfortunately, the available TSE data cannot be interpolated to be compared with the RG and with MC estimates in the vicinity of TCP. To clarify this issue, improved simulations by at least one of the three methods—MC, TSE and the SC-LPA RG—would be desirable.

## 6. Conclusion

In this paper the SC-LPA RG approach developed in [15, 22] where it was applied to the description of critical behaviour in 3d lattice models has been extended to additionally describe TCP and FOPTs that appear in the most complete version of the Landau-Ginzburg model with polynomial interaction of the sixth order ( $\phi^6$  model) [28], thus completing the RG solution of the model. The sc BCM has been chosen to validate the approach because, on the one hand, its MF solution contains all salient features of the  $\phi^6$  model [4], on the other hand, being a spin-lattice model, it has been extensively studied by such reliable techniques as the exact MC simulations and the TSE [33, 30, 34, 35, 4] so a wealth of quantitative data are available for quantitative comparison.

It has been found that the SC-LPA RG approach describes the continuous transitions in BCM in zero external field with the same accuracy ( $\leq 0.6\%$ ) as in previous studies [15, 22]; in particular, the TCP parameters have been determined with errors  $\lesssim 0.2\%$  and the classical tricritical exponents have been reproduced exactly in the LPA RG.

The most important advancements in comparison with [15, 22] concern the description of FOPTs. In the only systematic quantitative study of BCM FOPTs in [4] carried out by TSE method the authors found that at the level of truncation of TSE adopted by them the FOPT temperatures were systematically underestimated. The authors assessed the discrepancies quantitatively via comparison with reliably determined critical temperatures. In the present study it has been shown that the temperatures calculated by SC-LPA RG technique are close to those that would be obtained if the TSE predictions were corrected on the discrepancies. Also for the diagram the transition temperature versus non-ordering density the RG data seems to be more accurate and consistent than the TSE ones. Thus, it seems that at present the SC-LPA RG approach gives more accurate and complete description of FOPTs in 3d lattice models of the Landau-Ginzburg type than is currently accessible to alternative approaches. However, in the absence of internal criteria on the equations accuracy, more extended TSE and/or more accurate MC data would be desirable to confirm the above statement.

It is pertinent to point out that the main advantage of the proposed RG approach is its computational simplicity. While MC simulations in principle are capable of producing more reliable and accurate results, the description of one critical point may require the use of five Linux clusters and still some quantities can be determined inaccurately [5, 15]. Besides, the treatment of pair interactions of long extent is a challenging task for both



MC and TSE methods. The SC-LPA RG equations, in contrast, can be easily solved on virtually any computer irrespective of the extent of the pair interactions and the complete phase diagram can be drawn with much less effort than in the MC approach. The latter, however, may be needed to validate the RG data by checking their accuracy at a few points.

The accurate quantitative description of FOPTs achieved in the SC-LPA RG approach lends support to the underlying picture of the RG flow. The latter has been described with resort to the GBE that can be straightforwardly derived from the SC-LPA RG equation in the scalar case. It has been shown that by analogy with the well-studied example of the IRIM [48, 45], FOPTs in the short-range models should correspond to the discontinuous shock wave solutions of GBE. It has been argued that such solutions that normally do not appear in the viscous equation should be observable in the equations originating from the LPA RG case when the viscosity and its derivative turn to zero at the end of renormalization. Though a rigorous proof of this statement has not been given, in numerical simulations it has been satisfied within the accuracy of the calculations  $O(10^{-6})$  which should be sufficient for an approximate theory.

The RG description of FOPTs in IRIM and in the short range models had not revealed any qualitative difference between the two cases which in particular means that unlike in the case of critical phenomena, the Landau mean field theory is qualitatively correct in FOPT case. This may be helpful in clarifying the controversial issue of the discontinuity fixed point discussed in [50, 42, 20, 43, 9]. In the Landau theory thermodynamic system is considered to be of arbitrary dimension, spatial correlations between the system constituents are absent and the scaling does not take place [28]. Therefore, the use in the description of FOPTs of the scaling relations, especially those that include the dimensionality [20], can be misleading.

To sum up, the SC-LPA RG equations due to their simplicity, numerical accuracy and versatility may serve as a viable alternative to existing approaches in the approximate description of phase transitions in 3d lattice models with local interactions.

## Acknowledgments

This research was supported by the National Academy of Sciences of Ukraine under contract No. 22/20-H. I am indebted to Hugues Dreyssé for his support and encouragement. I express my gratitude to Université de Strasbourg and IPCMS for their hospitality and to René Monnier for interest in the work.

- [1] Bagnuls C, Bervillier C, Meiron D I and Nickel B G 1987 *Phys. Rev. B* **35** 3585–3607
- [2] Binder K 1986 *Monte Carlo Methods in Statistical Physics (Topics in Current Physics vol 7)* ed Binder K (Heidelberg: Springer-Verlag) p 1
- [3] Butera P and Comi M 2000 *Phys. Rev. B* **62** 14837–14843
- [4] Butera P and Pernici M 2018 *Physica A* **507** 22–66
- [5] Ferrenberg A M, Xu J and Landau D P 2018 *Phys. Rev. E* **97** 043301
- [6] Blume M 1966 *Phys. Rev.* **141** 517–524
- [7] Capel H W 1966 *Physica* **32** 966–988
- [8] Ng W M and Barry J H 1978 *Phys. Rev. B* **17** 3675–3683

- [9] Parola A, Pini D and Reatto L 1993 *Phys. Rev. E* **48** 3321–3332
- [10] Tokar V I 1997 *Comput. Mater. Sci.* **8** 8–15
- [11] Grollau S, Kierlik E, Rosinberg M L and Tarjus G 2001 *Phys. Rev. E* **63** 041111
- [12] Machado T and Dupuis N 2010 *Phys. Rev. E* **82**(4) 041128
- [13] Tan T L and Johnson D D 2011 *Phys. Rev. B* **83** 144427
- [14] Parola A and Reatto L 2012 *Mol. Phys.* **110** 2859–2882
- [15] Tokar V I 2021 *J. Stat. Mech.: Theory Exp.* **2021** 013215
- [16] Bagnuls C and Bervillier C 2001 *Phys. Rep.* **348** 91–157
- [17] Berges J, Tetradis N and Wetterich C 2002 *Phys. Rep.* **363** 223 – 386
- [18] Lundow P, Markström K and Rosengren A 2009 *Phil. Mag.* **89** 2009–2042
- [19] Wilson K G and Kogut J 1974 *Phys. Rep.* **12** 75–199
- [20] Fisher M E and Berker A N 1982 *Phys. Rev. B* **26** 2507–2513
- [21] Tokar V I 1984 *Phys. Lett. A* **104** 135–139
- [22] Tokar V I 2019 Calculation of non-universal thermodynamic quantities within self-consistent non-perturbative functional renormalization group approach (*Preprint* 1904.10338)
- [23] Riedel E K and Wegner F J 1972 *Phys. Rev. Lett.* **29** 349–352
- [24] Nicoll J F, Chang T S and Stanley H E 1976 *Phys. Rev. A* **13** 1251–1264
- [25] Caillol J M 2012 *Nucl. Phys. B* **855** 854–884
- [26] Bervillier C 2013 *Nucl. Phys. B* **876** 587
- [27] Doyle J and Englefield M J 1990 *IMA J. Appl. Math.* **44** 145–153
- [28] Landau L and Lifshitz E 1980 *Statistical Physics* v. 5 (Elsevier Science)
- [29] Deserno M 1997 *Phys. Rev. E* **56** 5204–5210
- [30] Özkan A, Seferoğlu N and Kutlu B 2006 *Physica A* **362** 327–337
- [31] Tokar V I 1985 *Phys. Lett. A* **110** 453–456
- [32] Blume M, Emery V J and Griffiths R B 1971 *Phys. Rev. A* **4** 1071–1077
- [33] Deng Y and Blöte H W J 2004 *Phys. Rev. E* **70** 056132
- [34] Hasenbusch M 2010 *Phys. Rev. B* **82** 174433
- [35] Fytas N G and Theodorakis P E 2013 *EPJ B* **86** 30
- [36] Riedel E K 1972 *Phys. Rev. Lett.* **28** 675–678
- [37] Pelissetto A and Vicari E 2002 *Phys. Rep.* **368** 549–727
- [38] Stinchcombe R 1984 *Phase Transitions and Critical Phenomena* vol 7 ed Domb C and Lebowitz J (London: Academic Press) p 152
- [39] Deng Y and Blöte H W J 2004 *Phys. Rev. E* **70**(4) 046111
- [40] Wegner F J 1972 *Phys. Rev. B* **5** 4529–4536
- [41] Deng Y and Blöte H W J 2003 *Phys. Rev. E* **68** 036125
- [42] Zia R K P 1981 *Z. Phys. B* **41** 129–138
- [43] Privman V and Schulman L 1982 *J. Stat. Phys.* **29** 205–229
- [44] Whitham G 2011 *Linear and Nonlinear Waves* Pure and Applied Mathematics: A Wiley Series of Texts, Monographs and Tracts (Wiley)
- [45] Choquard P and Wagner J 2004 *Journal of Statistical Physics* **116** 843–853
- [46] Lorenzoni P and Moro A 2019 *Phys. Rev. E* **100** 022103
- [47] Debnath L 2012 Conservation laws and shock waves *Nonlinear Partial Differential Equations for Scientists and Engineers* (Boston: Birkhäuser) pp 257–281
- [48] Brankov J G and Zagrebnov V A 1983 *J. Phys. A Math. Gen.* **16** 2217–2224
- [49] Salinas S 2001 *Introduction to Statistical Physics* Graduate Texts in Contemporary Physics (Springer New York)
- [50] Nienhuis B and Nauenberg M 1975 *Phys. Rev. Lett.* **35** 477–479
- [51] Burkhardt T W and Knops H J F 1977 *Phys. Rev. B* **15** 1602–1605
- [52] Wilson W G and Vause C A 1987 *Phys. Rev. B* **36** 587–593